Article

Cell Systems

Molecular-Level Tuning of Cellular Autonomy Controls the Collective Behaviors of Cell Populations

Graphical Abstract

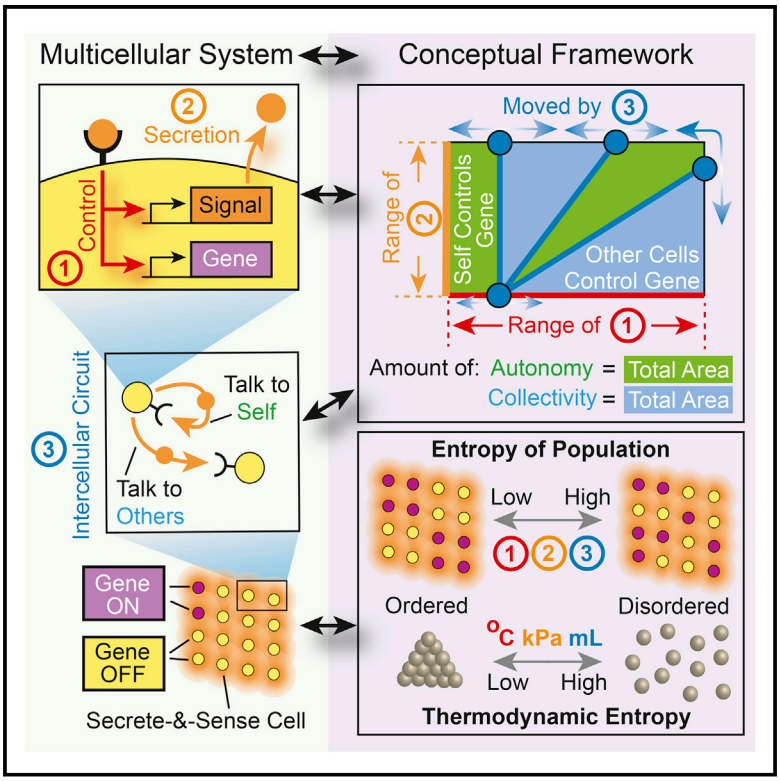

Authors

Théo Maire, Hyun Youk

Correspondence

h.youk@tudelft.nl

In Brief

Maire and Youk develop a conceptual framework for understanding the unicellular and multicellular control of gene expression for a ubiquitous class of cells that secretes and senses a signaling molecule. They use geometric means to quantify the amounts of autonomy and collectivity of cells and then connect these to the total number and orderliness of spatial patterns that a population of cells can form by introducing a concept of "entropy of population."

Highlights

- A theory links secrete-and-sense cells' genetic circuits to multicellular behaviors
- Degrees of autonomy and collectiveness are quantifiable and tunable
- "Phenotype diagrams" geometrize trade-offs between cells' autonomy and collectivity
- "Entropy of population" measures the population's ability to form spatial patterns

Maire & Youk, 2015, Cell Systems *1*, 349–360
November 25, 2015
http://dx.doi.org/10.1016/j.cels.2015.10.012

CellPress

Cell Systems
Article

Molecular-Level Tuning of Cellular Autonomy Controls the Collective Behaviors of Cell Populations

Théo Maire[1,2,3] and Hyun Youk[2,3,*]
[1]Department of Biology, École Normale Supérieure, Paris 75005, France
[2]Department of Bionanoscience
[3]Kavli Institute of Nanoscience
Delft University of Technology, Delft 2628, the Netherlands
*Correspondence: h.youk@tudelft.nl
http://dx.doi.org/10.1016/j.cels.2015.10.012

SUMMARY

A rigorous understanding of how multicellular behaviors arise from the actions of single cells requires quantitative frameworks that bridge the gap between genetic circuits, the arrangement of cells in space, and population-level behaviors. Here, we provide such a framework for a ubiquitous class of multicellular systems—namely, "secrete-and-sense cells" that communicate by secreting and sensing a signaling molecule. By using formal, mathematical arguments and introducing the concept of a phenotype diagram, we show how these cells tune their degrees of autonomous and collective behavior to realize distinct single-cell and population-level phenotypes; these phenomena have biological analogs, such as quorum sensing or paracrine signaling. We also define the "entropy of population," a measurement of the number of arrangements that a population of cells can assume, and demonstrate how a decrease in the entropy of population accompanies the formation of ordered spatial patterns. Our conceptual framework ties together diverse systems, including tissues and microbes, with common principles.

INTRODUCTION

Intuition tells us that if each cell behaves freely without being influenced by its neighbors, then a population of such autonomous cells would likely behave in a highly uncoordinated manner. On the other hand, if cells strongly influence each other by communicating with one another, then we would expect that a population of such cells would likely behave in a highly coordinated and collective manner. Because removing individual cells' autonomy both shapes the space of possible behaviors that a group of cells can have and limits it, cells likely have more ways to be uncoordinated than to be coordinated with one another. These qualitative and often loosely defined notions about communication among cells are deeply ingrained in our conventional thinking of multicellular behaviors such as the development of embryos, functioning of tissues, and microbes collectively fighting for their survival (Martinez Arias and Stewart, 2002), but many multicellular systems are too complex and involve too many parts (e.g., genetic circuits with many parts, cells at many different locations) for us to use intuition alone to understand and trace the steps that lead to their behaviors (Mehta and Gregor, 2010; Perrimon and Barkai, 2011; Markson and Elowitz, 2014). Casting these loose ideas in a rigorous mathematical framework that connects genetic circuits inside cells to population-level behaviors is crucial for understanding how genetic circuits and cell-cell communication yield multicellular behaviors. Such frameworks would define and quantify the amount of cell's freedom, the amount of cells' collectiveness, and the potential trade-off between the two. They may also provide common quantitative metrics and concepts that we can apply to many different multicellular systems.

Motivated by these considerations, this paper focuses on how cells use their genetic circuits and cell-cell communication to tune their "degree of autonomy" in order to coordinate their gene expression levels with one another. In particular, we focus on a ubiquitous class of multicellular system: a group of cells that secretes and senses one type of signaling molecule that we call "secrete-and-sense cells" (Figure 1A) (Youk and Lim, 2014). A secrete-and-sense cell can signal to itself (self-signaling) as well as to other cells (neighbor signaling) because it has a receptor that binds the signaling molecule secreted by both itself and its identical neighbors (Figure 1B) (Youk and Lim, 2014; Savir et al., 2012). Secrete-and-sense cells exist in diverse organisms. A special and perhaps the most well-known form of secrete-and-sense cells, called "quorum sensing cells," is abundant in the microbial world (Ng and Bassler, 2009). Quorum sensing cells maximize their neighbor-signaling ability while minimizing their self-signaling ability by, for example, having receptors with a very low binding affinity for the signaling molecule. Thus, only when there is a sufficiently high density of cells, which results in a high density of the secreted signaling molecule, can the cells capture enough signaling molecules to turn ON their genes. Another special form of secrete-and-sense cells, called "autocrine cells," is abundant in the metazoan world (Sporn and Todaro, 1980). Unlike the quorum sensing cells, autocrine cells maximize their self-signaling ability while minimizing their neighbor-signaling ability by, for example, producing large

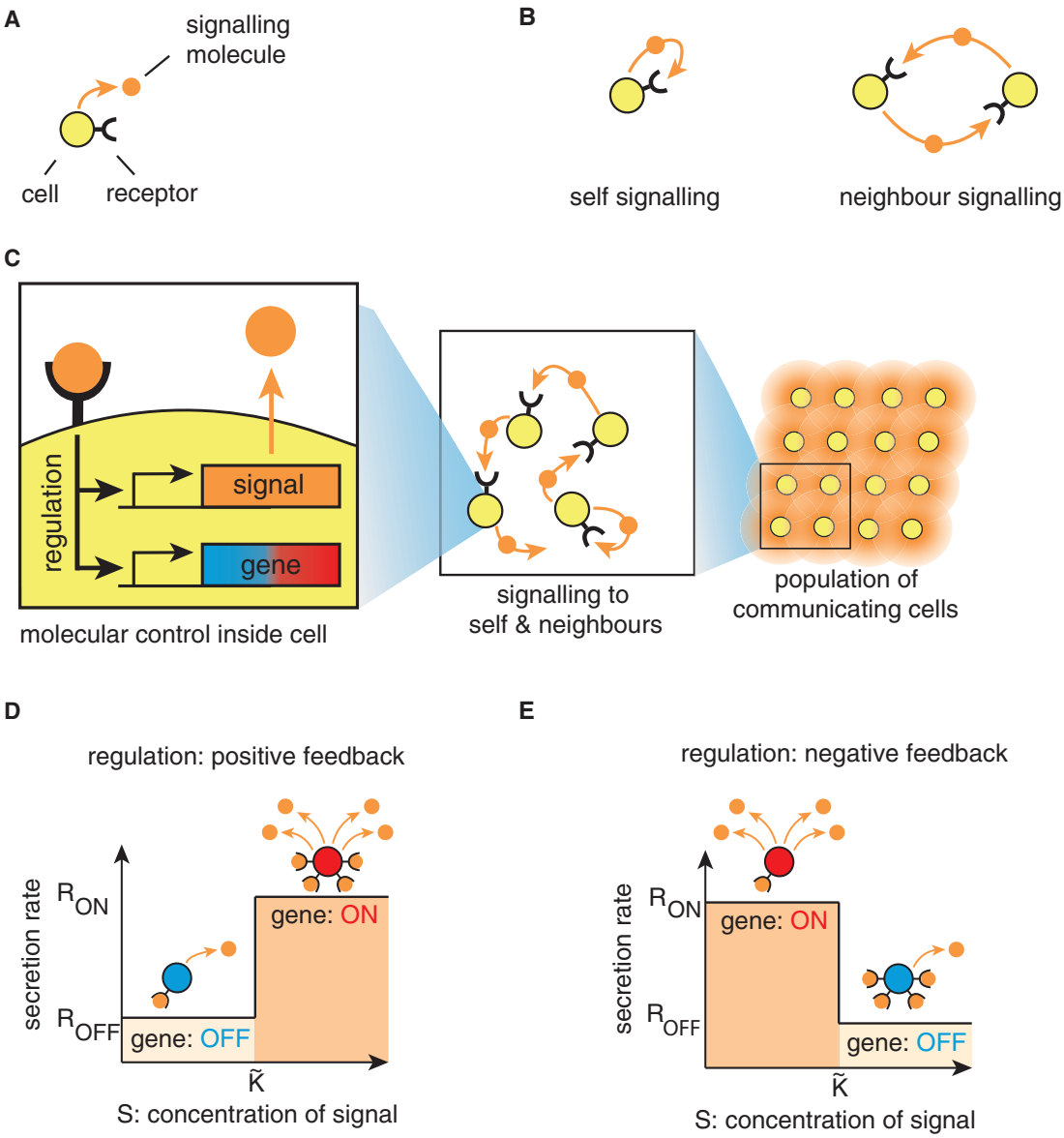

Figure 1. From Molecules to Populations of Cells: Our Bottom-Up Approach

(A) A secrete-and-sense cell.

(B) Secrete-and-sense cell can signal to itself (self-signaling) and signal to its neighboring cells (neighbor signaling).

(C) Outline of our bottom-up approach.

(D) Positive feedback regulation. If the cell senses less than the threshold concentration $\tilde{K}$ of the signaling molecule, it is in the OFF state and secretes the signaling molecule at a constant rate R_{OFF}; otherwise the cell is ON and secretes the molecule at the maximal rate R_{ON}.

(E) The intracellular regulation (left in C) can be a negative feedback.

amounts of receptors that bind the signaling molecule. Thus, an autocrine cell can easily capture a molecule it had just secreted before the molecule travels far away from the cell. Many microbial and metazoan secrete-and-sense cells, however, have equally dominant self- and neighbor-signaling abilities (Youk and Lim, 2014). Examples of secrete-and-sense cells, each with varying degrees of self- and neighbor-signaling abilities, include the soil amoebae *D. discoideum* that secrete and sense cAMP to aggregate together (Sgro et al., 2015; Gregor et al., 2010), cells within the embryos of *D. melanogaster* that regulate their fates by secreting and sensing "wingless" (Hooper, 1994), T cells that secrete and sense interleukin-2 (IL-2) to regulate their population density (Hart and Alon, 2013; Hart et al., 2014), the marine bacteria *Vibrio harveyi* that quorum sense to collectively generate light (Long et al., 2009), mammary cells whose misregulated secreting and sensing of IL-6 is a key step in carcinogenesis (Sansone et al., 2007), and *E. coli* cells that use synthetic genetic circuits to quorum sense and form diverse spatial patterns (You et al., 2004; Tanouchi et al., 2008; Song et al., 2009; Pai and You, 2009; Payne et al., 2013). A recent work has

revealed that a 2D lattice of hair follicles underneath the skin, despite being macroscopic organs, can also act as point-like secrete-and-sense cells that collectively regenerate hairs (Chen et al., 2015). The ubiquity of secrete-and-sense cells and the fact that despite their diversity they use common types of genetic circuits to regulate their secretion and sensing (Youk and Lim, 2014) make these cells ideal beds for developing a general theory.

Here we use a bottom-up approach to derive such a general theory for secrete-and-sense cells. We first show how an isolated secrete-and-sense cell uses its self-signaling (Figure 1B) to regulate its own gene expression. We then show how this cell's autonomous gene regulations (which we call "autonomous behaviors") morph into gene regulations that depend on the neighbors' signaling molecules (which we call "collective behaviors") as we increase the number of neighboring cells and the strength of cell-cell communication. In this process, we define and quantify the cells' degree of autonomy, degree of collectiveness, and the trade-off between the two by representing them as geometric shapes in a "phenotype diagram." We complete our theory by introducing a concept of "entropy of population" that quantifies the consequences of tuning the degree of each cell's autonomy on the whole population. Finally, we give examples of how one can apply our theoretical framework to better understand and engineer secrete-and-sense cells found in nature.

RESULTS

Autonomous Behaviors of an Isolated Secrete-and-Sense Cell

We first derive in detail how an isolated secrete-and-sense cell senses its own signaling molecule to regulate its genes. An isolated cell signals only to itself (self-signaling in Figure 1B) (Fallon and Lauffenburger, 2000). The concentration of the signaling molecule outside the cell controls the cell's secretion rate of the signaling molecule. Binding of the molecule to the cell's receptor triggers a cascade of molecular events inside the cell (Figure 1C) that either increases (through a positive feedback, Figure 1D) or decreases (through a negative feedback, Figure 1E) the secretion rate by regulating a gene that encodes the signaling molecule (orange box in Figure 1C) (Youk and Lim, 2014). This binding usually also controls one or more "reporter genes" (blue-red box in Figure 1C) that regulate signaling pathways inside the cell (e.g., a master regulator of the stem cell's fate) (Hart et al., 2014; Sgro et al., 2015, Gregor et al., 2010). A sigmoidal function usually describes the cell's secretion rate and the reporter gene's expression level as a function of the signaling molecule's concentration. In many secrete-and-sense cells found in nature, a step function closely approximates the sigmoidal function (Figures 1D and 1E) (Dayarian et al., 2009; Pai et al., 2014; Hart et al., 2014; Youk and Lim, 2014; Gregor et al., 2010; Hermsen et al., 2010; Hart et al., 2012). That is, the cell's reporter gene is restricted to be either ON or OFF. An ON cell has a secretion rate R_{ON}, and an OFF cell has a secretion rate R_{OFF}. R_{ON} is larger than R_{OFF}. The cell switches between the two states at a threshold concentration $\widetilde{K}$ (Figures 1D and 1E). The threshold concentration can be tuned, for example, by changing the expression level of the receptor or the receptor's binding affinity for the signaling molecule (Pai and You, 2009; Youk and Lim, 2014). For simplicity, we treat the cell to be point like. The concentration (denoted S) of the signaling molecule with a diffusion constant D and a degradation rate γ, at a distance r from the cell is governed by the 2D diffusion equation:

$$\frac{\partial S}{\partial t} = \underbrace{D\nabla^2 S}_{\text{diffusion}} - \underbrace{\gamma S}_{\text{degradation}} + \underbrace{R_O \delta(r)}_{\text{secretion}}. \qquad \text{(Equation 1)}$$

Here R_O is the secretion rate (equal to either R_{OFF} or R_{ON}), and $\delta(r)$ is 1 on the cell ($r = 0$) and zero everywhere else ($r > 0$). The degradation term can represent both a passive degradation of the signaling molecule (i.e., the molecule stochastically degrades) and an active degradation of the molecule by a protease that the cell may secrete at a constant rate. A typical cell repeatedly measures a fluctuating concentration over a long time, averages these multiple measurements, and then uses the average concentration to regulate its genes (Lalanne and François, 2015; Gregor et al., 2007; Govern and ten Wolde, 2012). Since the concentration usually reaches a steady state much faster than the time taken for this averaging, we can focus on how the steady-state concentration regulates the cell's behavior. The steady-state concentration in 2D forms a gradient that exponentially decays away from the cell:

$$S(r) = S_O exp\left(\frac{-r}{\lambda}\right). \qquad \text{(Equation 2)}$$

Here S_O is the concentration on the cell's surface. It is proportional to the secretion rate R_{ON} when the cell is ON (then we define $S_O \equiv \widetilde{S}_{ON}$) and to R_{OFF} when the cell is OFF (then we define $S_O \equiv \widetilde{S}_{OFF}$). $\lambda \equiv \sqrt{D/\gamma}$ is the typical distance that a signaling molecule travels before decaying. Thus, we can consider Equation 2 to describe a circular "cloud" of molecules, with radius λ, centered about the cell (Figure 2A). The cell senses the molecules in this cloud. Here we are assuming that the time taken for the secreted signaling molecules to reach a steady-state level (i.e., time taken to build the cloud) is much shorter than the time taken for the cell to determine the concentration and then regulating its genes in response to it. To make meaningful comparisons between the different terms, we divide all concentration terms by the OFF state's concentration $\widetilde{S}_{OFF}$:

$$\begin{cases} K = \dfrac{\widetilde{K}}{\widetilde{S}_{OFF}} \\ S_{ON} = \dfrac{\widetilde{S}_{ON}}{\widetilde{S}_{OFF}} \\ \widetilde{S}_{OFF} = 1 \end{cases}. \qquad \text{(Equation 3)}$$

Thus, we now measure all concentrations relative to $\widetilde{S}_{OFF}$ (thus $\widetilde{S}_{OFF} = 1$). Recast in these rescaled terms, S_{ON} is the concentration on the surface of the ON cell, whereas 1 is the concentration on the surface of the OFF cell. From Equation 3, we see that S_{ON} and K are the only freely tunable parameters for the cell. Since the cell's state (ON or OFF) depends only on comparing the threshold concentration K with the concentration on the cell surface (Figures 1D and 1E), a function that compares these two values, that we call "phenotype function,"

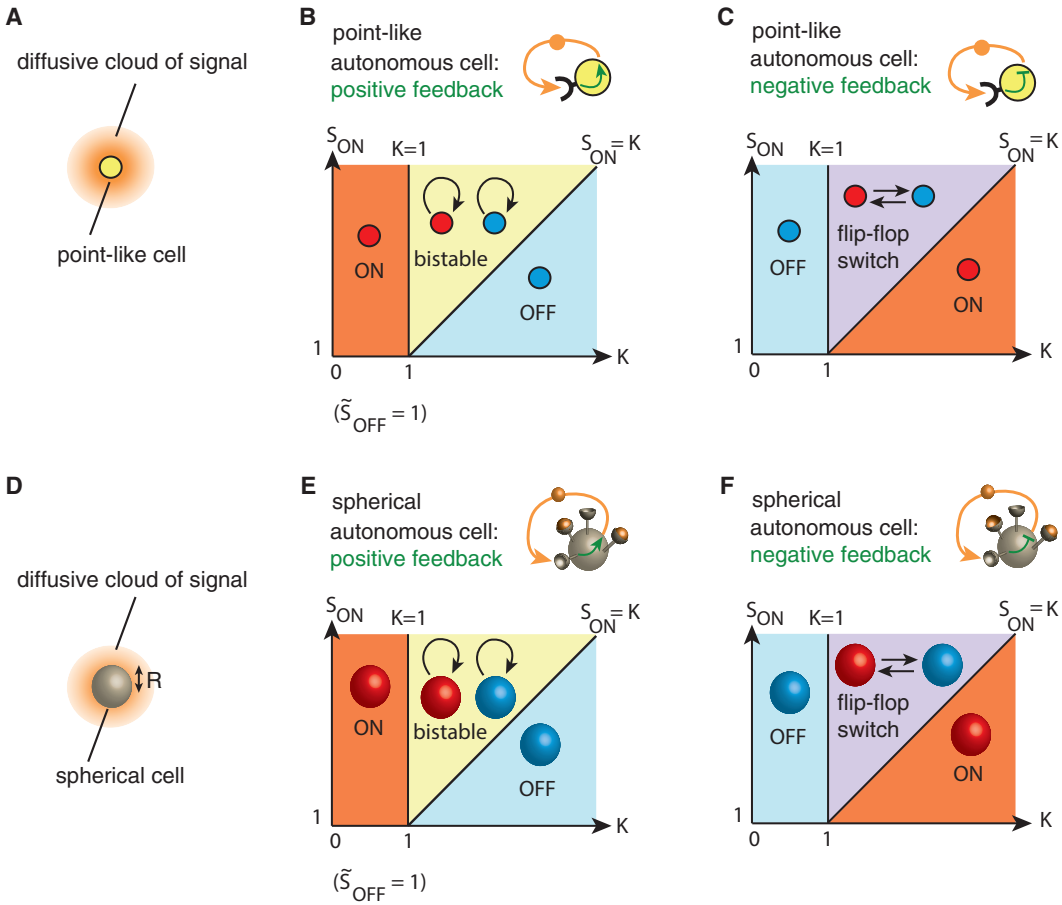

Figure 2. Autonomous Behaviors of an Isolated Cell

(A) An isolated point-like secrete-and-sense cell surrounded by a diffusive cloud of the signaling molecule. The decay length λ (Equation 2) is the radius of this diffusive cloud.

(B) Phenotype diagram of an isolated point-like cell with the positive feedback regulation.

(C) Phenotype diagram of an isolated point-like cell with the negative feedback regulation.

(D) An isolated spherical cell with radius *R* surrounded by a diffusive cloud of the signaling molecule.

(E) Phenotype diagram of an isolated spherical cell with the positive feedback regulation.

(F) Phenotype diagram of an isolated spherical cell with the negative feedback regulation.

would determine what the cell will do next (either maintain or change its current ON/OFF state). Since the concentration on the cell surface is either 1 or S_{ON}, we have two phenotype functions, φ_{OFF} and φ_{ON}:

$$\begin{cases} \varphi_{OFF}(K, S_{ON}) = 1 - K \\ \varphi_{ON}(K, S_{ON}) = S_{ON} - K \end{cases}. \quad \text{(Equation 4)}$$

For both the positive and the negative feedbacks, the sign of φ_{OFF} determines what the OFF cell will do next (remain OFF or turn ON), while the sign of φ_{ON} determines what the ON cell will do next (remain ON or turn OFF). Thus, the signs of both functions determine all possible autonomous behaviors ("phenotypes") of the cell. The possible combinations for the signs of φ_{OFF} and φ_{ON} are as follows:

$$\begin{cases} (1)\ \varphi_{OFF} > 0 \text{ and } \varphi_{ON} > 0 \\ (2)\ \varphi_{OFF} < 0 \text{ and } \varphi_{ON} > 0 \\ (3)\ \varphi_{OFF} < 0 \text{ and } \varphi_{ON} < 0 \end{cases}. \quad \text{(Equation 5)}$$

The scenario in which $\varphi_{OFF} > 0$ and $\varphi_{ON} < 0$ cannot occur because the secretion rate of the ON cell (R_{ON}) is larger than the secretion rate of the OFF cell (R_{OFF}). Thus, the concentration on the surface of the ON cell (S_{ON}) is larger than that of the OFF cell ($\tilde{S}_{OFF} = 1$). Thus, $\varphi_{ON} > \varphi_{OFF}$, and hence, we cannot simultaneously have $\varphi_{OFF} > 0$ and $\varphi_{ON} < 0$. For both the positive and negative feedback regulation, the above three conditions split the plane spanned by K and S_{ON} into three regions (Figures 2B and 2C). Each region represents a distinct phenotype of the cell. Thus, we call the resulting two diagrams, one for the positive feedback (Figure 2B) and the other for the negative feedback (Figure 2C), "phenotype diagrams." We deduce the phenotypes represented by each region from the input-output step functions (Figures 1D and 1E). A cell with the positive feedback and a cell with the negative feedback have two phenotypes in common. First, the cell turns itself ON and stays ON due to self-signaling (ON region in Figures 2B and 2C). Second, the cell's self-signal is insufficient to maintain itself ON so the

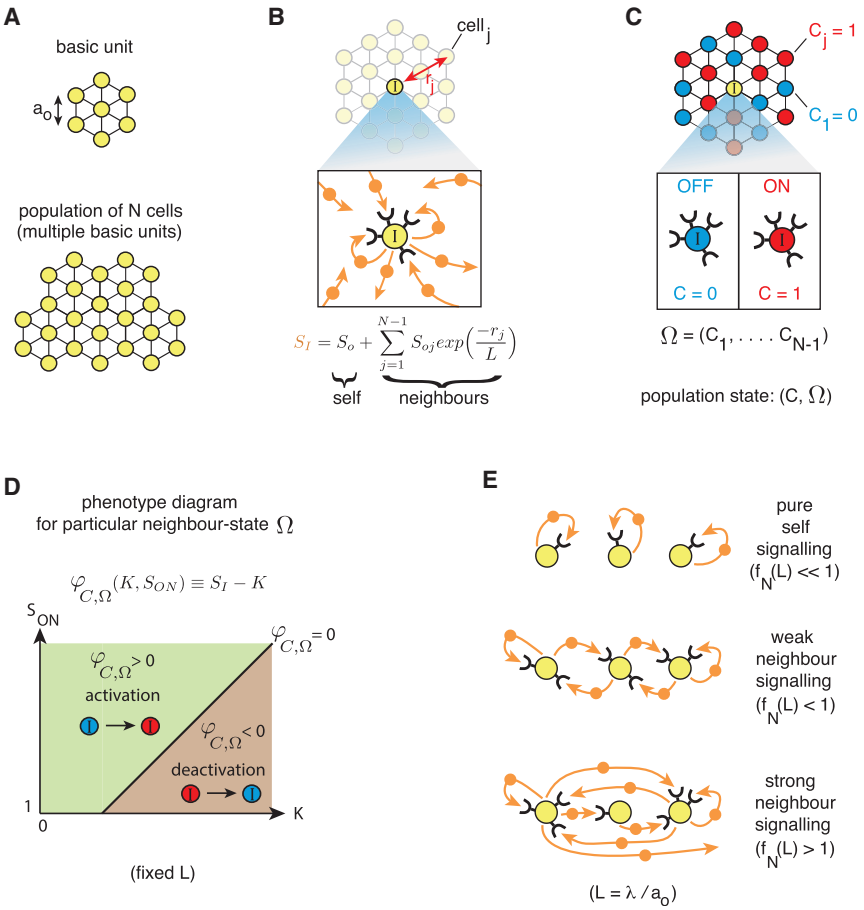

Figure 3. Quantifying Degrees of Autonomy and of Collectiveness

(A) A basic unit of seven cells on a regular hexagonal lattice with an edge length a_O (upper). Adjoining multiple basic units forms a population of N cells (lower).

(B) Pick any cell and call it cell-I (I for individual). We focus on cell-I's loss of autonomy as we tune its communication with all the other cells. S_I is the concentration of the signaling molecule on cell-I. The signaling length L is the distance that the signal travels before decaying.

(C) Population state is denoted by a string of 2^N binary digits: (C, Ω), where C is cell-I's state ($C = 0$ if cell-I is OFF, $C = 1$ if cell-I is ON) and Ω is the state of each of the N-1 neighboring cells.

(D) Phenotype diagram of cells with the positive feedback for a particular population state (C, Ω) and a fixed signaling length L.

(E) Tuning the signaling strength $f_N(L)$ (Equation 7) yields three regimes of cell-cell signaling.

cell remains OFF (OFF region in Figures 2B and 2C). In addition, the positive feedback enables a bistable phenotype (ON & OFF region in Figure 2B) in which the cell can either stay ON or stay OFF, depending on its past history. The bistable cell can switch between ON and OFF due to external perturbations and stochastic silencing or activation of its secretion. In the case of the negative feedback, the cell can flip back and forth between being ON and OFF over time. This occurs only if the molecule degrades sufficiently fast and its concentration reaches the steady state much faster than the cell can toggle between ON and OFF. The phenotype diagrams (Figures 2B and 2C) are geometric blueprints that tell us how the cell should tune the key parameters, K and S_{ON}, to realize these distinct phenotypes.

If the cell were a 3D sphere of radius R instead of being a point (Figure 2D), we would need to solve the 3D diffusion equation instead of Equation 1 to obtain the steady-state concentration around the cell in 3D. We have performed this calculation (see Supplemental Theoretical Procedures) and have found that the cell's radius R does not affect the ratio of $\widetilde{S}_{ON}$ to $\widetilde{S}_{OFF}$ (Figure S1). Thus, if we measure the concentration in units of $\widetilde{S}_{OFF}$ (i.e., $\widetilde{S}_{OFF} = 1$) through Equation 3, then S_{ON} is independent of how big the spherical cell is. As a result, we obtain phenotype diagrams for a spherical cell (Figures 2E and 2F) that are identical to the phenotype diagrams of the point-like cell.

Entangled Web of Cell-Cell Communications in a Population

We now present a general formalism to study a population with an arbitrary number of cells. We first define a "basic unit" (Figure 3A), which serves as our elementary building block of larger populations. It consists of identical secrete-and-sense cells at each corner of a hexagon with an edge length a_O. It also has a cell at its center (Figure 3A). To build a population of N cells, we repeatedly tile the basic unit next to each other (Figure 3A) (our framework is applicable to any polygon besides the hexagon). Our main idea is to pick any arbitrary cell in the population, call it "cell-I" ("I" for individual), and then analyze how its state (ON or OFF) changes as we tune its communication with all the other cells. We number all the other cells (the "neighbors"), from 1 to $N - 1$. The concentration S_I of the signaling molecule sensed by cell-I is the sum of the concentration of the molecule secreted by cell-I (denoted S_{self}) (Equation 2) and the concentration of the molecule secreted by all the other cells (denoted $S_{neighbors}$) (Figure 3B):

$$S_I = \underbrace{S_O}_{\text{due to self}\,(=S_{self})} + \underbrace{\sum_{j=1}^{N-1} S_{Oj} exp\left(\frac{-r_j}{L}\right)}_{\text{due to neighbors}\,\left(=S_{neighbors}\right)} . \qquad \text{(Equation 6)}$$

Here, r_j is the distance between a j^{th} cell and cell-I in units of the edge length a_O. $L \equiv \lambda / a_O$ is the "signaling length," which is the radius of the diffusive signal cloud (Figure 2A) in units of the edge length. The terms S_O and S_{Oj} depend on the state of cell-I and the j^{th} cell, respectively (i.e., they are either S_{ON} or 1).

To compute the concentration S_I sensed by cell-I, we need a system for keeping track of the state of every cell in the population. We let C represent cell-I's state (Figure 3C). $C = 1$ denotes an ON cell-I, whereas $C = 0$ denotes an OFF cell-I. Similarly, we let C_j denote the state of the j^{th} neighbor (Figure 3C). Then the

string $\Omega = (C_1, C_2,...,C_{N-1})$, which we call "neighbor state," denotes the state of all the neighbors. Moreover the string of N binary digits (C, Ω), which we call "population state," represents the state of the whole population. Since there are 2^N different population states, the concentration S_I has 2^N possible values (one for each possible value of (C, Ω)). This is a large number even for a small population size (e.g., for a population of N = 20 cells, 2^N is approximately 1 million). Our challenge then is to reduce this complexity, provide a rigorous description of cell-I's degree of autonomy, and reveal all possible behaviors of the population.

Phenotype Functions for Populations

If we know cell-I's behavior in each neighbor state, then we know how cell-I would behave under all possible neighbor states. First, we deduce cell-I's phenotypes for a fixed state of the neighbors (i.e., fix a value for Ω). For this neighbor state, we define a phenotype function: $\varphi_{C,\Omega}(K, S_{ON}, L) \equiv S_I - K$. To construct cell-I's phenotype diagram for this particular neighbor state, let us first fix the value of signaling length L so that we only need to consider how the values of (K, S_{ON}) affect the phenotype function. We note that the values of (K, S_{ON}) for which $\varphi_{C,\Omega} = 0$ form a straight line (Figure 3D). We call the region above this line an "activation region" (Figure 3D, green region). In this region, cell-I turns ON because it senses a concentration S_I that is above the threshold concentration K (i.e., $\varphi_{C,\Omega} > 0$). Below the line is the "deactivation region" (Figure 3D, brown region). In this region, cell-I turns OFF because it senses a concentration S_I that is below the threshold concentration K (i.e., $\varphi_{C,\Omega} < 0$). Repeating this procedure for every neighbor state in a population of N cells, we would obtain 2^N activation regions and deactivation regions. When we overlay all these regions onto one plane, we would obtain a full phenotype diagram that shows all possible behaviors of cell-I because it takes into account every possible state of the neighbors.

Main Design Principle: Self-Signaling Competes with Neighbor Signaling to Control the Cell's Autonomy

We have now established our formalism, but before applying it to a population of an arbitrary size, we now explain the main principle that gives rise to different phenotypes. Our idea is to compare the influence on cell-I by self-signaling with the neighbors' influence. First note that the neighbors have minimal influence on cell-I if all of them are OFF. This minimum concentration that the neighbors can create on cell-I is (by setting $S_{Oj} = 1$ for all neighbors in Equation 6):

$$f_N(L) = \sum_{j=1}^{N-1} exp(-r_j/L). \qquad \text{(Equation 7)}$$

For reasons we see shortly, we call $f_N(L)$ the "signaling strength" function. The maximum concentration that the neighbors can generate is $S_{ON} f_N(L)$, which is realized when all the neighbors are ON. The difference between the maximum and the minimum (denoted $\Delta S_{neighbours}$) represents the range of influence that the neighbors have on cell-I. Analogously, the difference between the maximum (S_{ON}) and the minimum concentration (1) generated by cell-I on itself (denoted ΔS_{self}) represents the range of influence that self-signaling has on cell-I. Specifically, having ΔS_{self} larger than $\Delta S_{neighbours}$ ($\Delta S_{self} > \Delta S_{neighbours}$) means that cell-I can sense more of its own signaling molecules than the neighbors' signaling molecules, just as an autocrine cell would. In this case, we find that the signaling strength $f_N(L)$ is less than one (Figure 3E). On the other hand, having ΔS_{self} smaller than $\Delta S_{neighbours}$ ($\Delta S_{self} < \Delta S_{neighbours}$) means that cell-I can sense more signals from its neighbors than from itself, just as a quorum-sensing cell would. In this case, we find that the signaling strength $f_N(L)$ is larger than one (Figure 3E). The two cases are separated by a "critical signaling length" L_c, whereby the influence of self and neighbors are exactly balanced (i.e., $f_N(L_c) = 1$).

To state in another way, self-signaling (thus autonomy) dominates when L is less than L_c, but signaling between cells (thus collectiveness) dominates when L is larger than L_c (Figure 3E). The critical signaling length L_c depends on the number of cells in the population. Crucially, we can always find a critical length for a population with any number of cells. This means that no matter how many cells form a population, cells can always adjust their signaling length L so that each cell has some degree of autonomy. From here on, we focus on cells with the positive feedback and not repeat our calculations for cells with the negative feedback because both regulations use our theoretical formalism in the same way.

Application of Our General Formalism to a Small Population: A Basic Population Unit

We now apply our formalism to a small population—the hexagonal basic unit (Figure 3A). We choose cell-I to be at the center of the hexagon and consider a scenario in which the signaling length L is shorter than the critical length L_c. Applying our formalism (see Experimental Procedures), we obtain a phenotype diagram with geometric regions that mark different phenotypes of cell-I (Figure 4A, right). It has three types of regions: activation regions, deactivation regions, and an autonomous bistable region.

The activation regions consist of several subregions. One is the autonomous ON region in which cell-I autonomously turns itself ON (Figure 4A, orange ON region). The others are neighbor-induced activation regions (Figure 4A, green regions denoted $\widetilde{An}$), in which cell-I turns ON only if there are at least n ON neighbors (Figure 4B).

The deactivation regions consist of several subregions as well. One is the autonomous OFF region in which cell-I turns itself OFF through self-signaling. The others are neighbor-induced deactivation regions (Figure 4A, brown regions denoted $\widetilde{Dn}$), in which cell-I turns OFF unless there is more than n ON neighbors (Figure 4B).

The autonomous bistable region (Figure 4A, yellow region denoted ON & OFF) represents the bistable ON & OFF phenotype that we previously described for the isolated cell. Here the cell is free to choose between being ON or OFF and is unable to listen to its neighbors.

Comparing the phenotype diagram of the isolated cell (Figure 4A, left) with that of the basic population unit (Figure 4A, right), we see that the global effect of cell-cell signaling is reducing the combined area of the three autonomy regions (Figure 4A, blue, yellow, orange regions) to make room for the neighbor-induced activation regions (the $\widetilde{An}$'s in Figure 4A) and neighbor-induced deactivation regions (the $\widetilde{Dn}$'s in

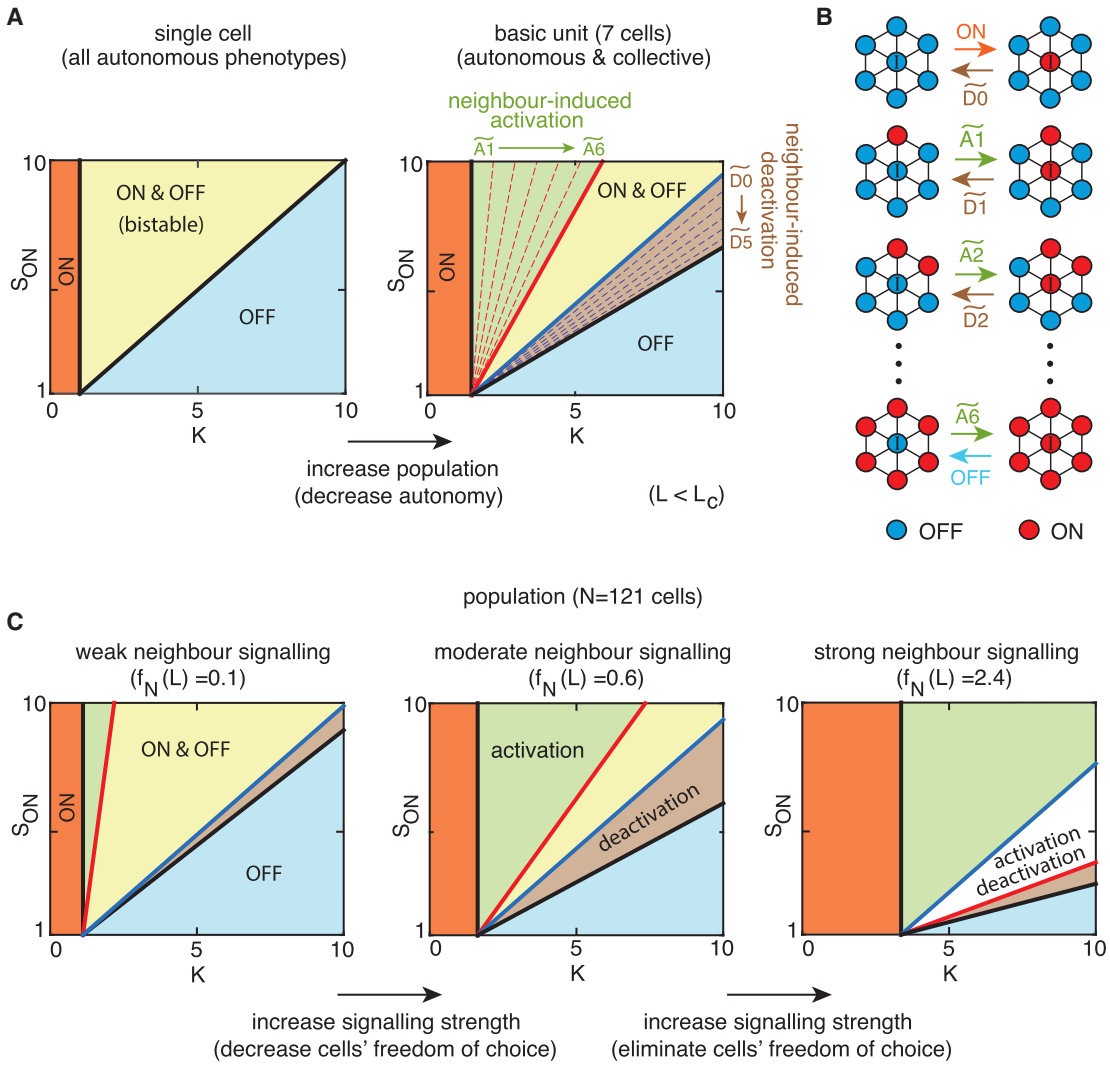

Figure 4. Populations with *N* Cells and Various Cell-Cell Signaling Strengths

(A) Phenotype diagrams for an isolated cell with the positive feedback (left) and the hexagonal basic unit with a positive feedback (right), $L = 0.4$ ($L_c \approx 0.56$). The neighbor-induced activation region is green, and the neighbor-induced deactivation region is brown. Equation 9 describes the boundary lines.

(B) Each region in the basic unit's phenotypic diagram (right, A) represents a state transition as shown here.

(C) Phenotype diagrams for a population with 121 cells (11 × 11 grid of cells) at different values of L, with $L_c \approx 0.47$. The neighbor-induced activation region is green, and the neighbor-induced deactivation region is brown. For $L > L_c$, the activation-deactivation region (white region) arises.

Figure 4A). Despite its reduction, the total area of the autonomy regions remains non-zero, meaning that cell-I can regulate its genes autonomously. Our analysis here shows that the combined area of the autonomy regions is a sensible and a quantitative representation of cells' degree of autonomy. The combined area of the regions representing neighbor-induced phenotypes quantifies the cells' degree of collectiveness.

If the basic unit consists of spherical cells of radius R, we obtain a phenotype diagram for the basic unit (Figure S1) that is essentially identical to that of the basic unit composed of point-like cells. The reason is that S_{ON} is independent of R if we measure all concentrations relative to $\widetilde{S}_{OFF}$ (i.e., $\widetilde{S}_{OFF} = 1$), as in the case of an isolated spherical cell (see Supplemental Experimental Procedures).

Application of Our General Formalism: Population of an Arbitrary Size

We now apply our formalism to the most general case: a population with N cells with a positive feedback. Thus, we can now allow populations to be of an arbitrarily large size. Applying our formalism (see Experimental Procedures), we obtain a phenotype diagram with distinct regions (Figure 4C) in which areas depend on the signaling strength $f_N(L)$.

When the signaling strength is very weak (i.e., $f_N(L) << 1$), there is a finite but nearly negligible signals from the neighbors. Thus, we obtain a phenotype diagram (Figure 4C, left) that is similar to that of the isolated cell (Figure 4A, left). The only difference is that the weak signals from the neighbors have reduced the area of the autonomous bistable region (Figure 4C, left, yellow ON & OFF

region) and the area of the autonomous OFF region (Figure 4C, left, blue OFF region). This contraction in the areas of the two regions makes room for two new regions: a neighbor-induced activation region (Figure 4C, left, green region) and a neighbor-induced deactivation region (Figure 4C, left, brown region). As we did in the case of the basic population unit, we see a decrease in each cell's degree of autonomy (i.e., decrease in combined areas of orange, yellow, and blue regions) and as a trade-off, a corresponding increase in the cells' degree of collectiveness (areas of the green and brown regions).

If we now increase the signaling length L but still keep it below the critical signaling length L_c (Figure 4C, middle), the neighbor-induced activation region further expands into and overtakes the autonomous bistable region (Figure 4C, middle, green invades into yellow). In addition, the neighbor-induced deactivation region further expands into and overtakes the autonomous OFF region (Figure 4C, middle, brown invades into blue). This further increases the cells' degree of collectiveness at the expense of the decrease in the degree of autonomy in the corresponding amount.

If we further increase the signaling length L, this time above the critical signaling length L_c (Figure 4C, right), the autonomous bistable region vanishes because the neighbor-induced activation region completely overtakes it. The neighbor-induced activation region also invades into the neighbor-induced deactivation region (i.e., green invades into brown region). Their merging results in the creation of a new phenotype region that we call "activation-deactivation region" (Figure 4C, right, white region). In this region, the neighbors collectively decide whether to activate or deactivate cell-I depending on which of the two is larger: the density of ON neighbors (leads to activation) or the density of OFF neighbors (leads to deactivation). Thus, we can think of this region as representing a multicellular bistable switch—a type of quorum sensing (Ng and Bassler, 2009; Pai et al., 2012; Mehta et al., 2009) that measures the density of ON/OFF cells and their local spatial distributions. It is the multicellular analog (i.e., dependent on neighbors) of the autonomous bistable switch (Figure 4A, yellow ON & OFF region). We see additional reasons later for why this reasoning makes sense when we analyze population-level dynamics enabled by the activation-deactivation region.

We note that while the cells can increase their signaling length L above the critical length L_c to eliminate their autonomous bistable region (Figure 4C, yellow region), the autonomous ON region (Figure 4C, orange region) and the autonomous OFF region (Figure 4C, blue region) still remain, but the cells in these two regions must solely remain ON or remain OFF, respectively. However, the cells in the autonomous bistable region may choose: either stay ON or stay OFF. Increasing the signaling length L gradually eliminates this freedom by making the autonomous bistable region vanish. Thus, while the cells' degree of autonomy remains non-zero when the signaling strength is above 1 (i.e., $f(L_c) > 1$), the cells' degree of autonomous choice (area of the yellow region) completely vanishes.

If we have a population of N spherical cells, we can still apply the formalism that we applied to the population of point-like cells. In fact, our calculations show that the phenotype diagrams for a population of N spherical cells are essentially identical to those of a population of N point-like cells (see Supplemental Theoretical Procedures). There are quantitative differences between the population of point-like and population of spherical cells. Namely, the radius R of the spherical cells affects the signaling strength function (denoted $f_{N,R}(L)$) and the concentration S_I sensed by cell-I (Figure S1). However, the signaling strength $f_{N,R}(L)$ of the spherical cells is still divided into the same three regimes (Figure 3E) as the point-like cells.

Entropy of Population Connects Unicellular Freedom with Population-Level Freedom

We now ask how the different unicellular phenotypes (Figure 4C) generate population-level dynamics (i.e., connecting middle to right in Figure 1C). To address this question, we first asked whether there are spatial arrangements of ON and OFF cells in which no cell's state (i.e., ON or OFF) would change over time. We say that such a population is in an equilibrium configuration. To search for such equilibrium configurations, we performed computer simulations in which we started with a randomly chosen initial arrangement of ON and OFF cells in a population (see Supplemental Theoretical Procedures). We then computed the concentration S_I for each cell (Equation 6). Then we checked whether any cell's state (ON or OFF) changed. If none of the cells' states changed, the initial population is in equilibrium. By repeating this process many times, each time with a different configuration of the population, we counted the number of equilibrium configurations that N cells can form with a particular value of (K, S_{ON}, L). We have done this for a wide range of values of (K, S_{ON}, L). To complement our simulations, we derived an analytical formula that estimates the number of equilibrium populations (denoted Ω_E) for each value of (K, S_{ON}, L) (see Supplemental Experimental Procedures). To meaningfully interpret and compare the Ω_E obtained by the two methods, we define entropy of population:

$$\sigma(K, S_{ON}, L) = \frac{\Omega_E}{2^N}. \qquad \text{(Equation 8)}$$

To see what this represents, note that 2^N is the total number of possible population states with N cells (Figure 3C). Thus, $\sigma = 1$ represents a maximal population-level disorder (population can be in any configuration) and maximal population-level freedom (any configuration is in equilibrium), while $\sigma = 1/2^N$ represents a minimal population-level disorder (everyone is in the same state) and minimal population-level freedom (only one configuration is in equilibrium). The entropy of population is thus a macroscopic (population-level) metric based on the microscopic (unicellular) parameters (K, S_{ON}, L) that measures the number of ways that stable gene expression levels (ON or OFF) can be assigned to cells at different locations. We found that the entropy of population determined by our simulations and formula closely agreed with each other for a wide range of values of (K, S_{ON}, L) (Figures 5A and 5B). We found that the entropy of population decreases when the cell-cell interaction strength $f_N(L)$ increases because cell-cell signaling to increases the cells' coordination (compare top and bottom in Figure 5B). We also see that the entropy of population is highest when the cells are in the autonomous bistable region (Figure 5B, yellow ON & OFF region). This makes sense because when every cell is completely free to choose its state the whole population can have the maximal number of

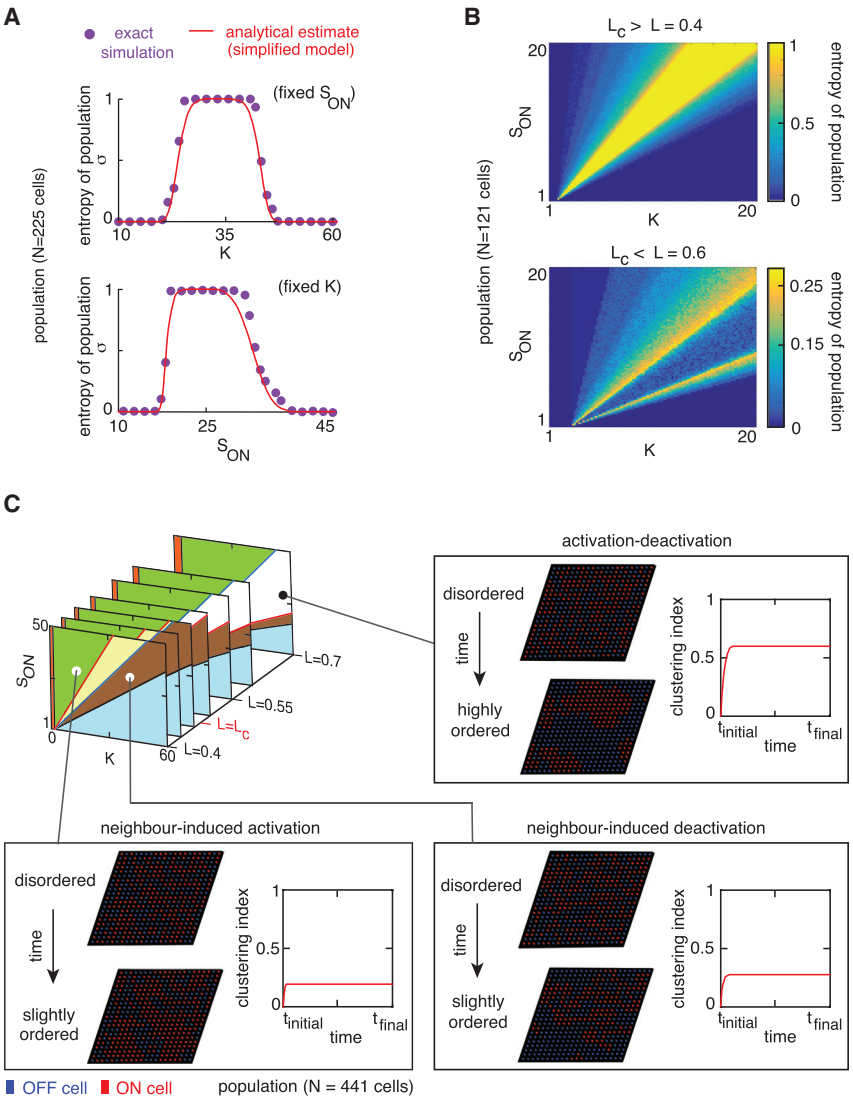

Figure 5. From Disorder to Order: Entropy of Population and Spatial Clustering Index

(A) The entropy of population (Equation 8) obtained by exact simulations (purple points) and by an analytical formula (red curve; see Supplemental Theoretical Procedures). Upper is for S_{ON} = 40, and the panel is for K = 45. Population size = 225 cells (grid of 15 × 15 cells). L = 0.4 ($L < L_c$).

(B) The entropy of population obtained by exact simulations for L = 0.4 (upper) and L = 0.6 (lower). The population size is 121 cells (grid of 11 × 11 cells). Sharp changes in the entropy of population occur at the boundaries between distinct phenotypic regions (compare with Figure 4C).

(C) Deterministic simulations of population dynamics. The population size is 441 cells (grid of 21 × 21 cells). OFF cells are blue, and ON cells are red. Initial and final configurations of populations with temporal changes in the clustering index I_M are shown. Results are shown for activation region (K = 15, S_{ON} = 30, L = 0.4), deactivation region (K = 36, S_{ON} = 30, L = 0.4), and the activation-deactivation region (K = 61, S_{ON} = 30, L = 0.7).

possible configurations. The entropy of population thus rigorously captures our qualitative notions about how unicellular autonomy is linked to cell-cell coordination at the population level.

Population-Level Dynamics: Self-Organization of Spatially Ordered Patterns from Spatially Disordered Populations

So far we have determined how a cell can dynamically change its state in response to signals from self and neighbors and the number of ways that populations can be in equilibrium. The final step of our bottom-up program (Figure 1C) is a determination of how cells within a population reach an equilibrium configuration. Population configurations that are not in equilibrium must, by definition, use cell-cell signaling to readjust the behavior of individual cells until the population reaches one of the equilibrium configurations. Development of spatial patterns, such as stripes and islands, occurs in real and quasi 2D systems such as tissues and embryos (Turing, 1952; Gregor et al., 2005; Ben-Zvi et al., 2008; Perrimon et al., 2012; Sprinzak et al., 2010). The general principles that govern how these spatial patterns form from secrete-and-sense cells have been elusive. To gain insights, we investigated whether ON and OFF cells that are randomly distributed over space can dynamically self-organize into a population with defined spatial patterns. To quantify the spatial ordering of cells, we define a "clustering index" I_M, motivated by a statistical metric called "Moran's I" (Moran, 1950; see Experimental Procedures). Our clustering index I_M quantifies how closely ON cells (and thus OFF cells) cluster together in space. The clustering index can be between 0 (spatially disordered state) and 1 (spatially ordered state) (Figure S2). As the clustering index approaches zero, ON and OFF cells become more randomly dispersed in space. As the clustering index approaches one, ON cells become more clustered together in one spatial region (e.g., island of ON cells surrounded by a sea of OFF cells).

For each region of the phenotype diagrams (Figure 4C), we used two types of simulations to determine how an initially randomly distributed cells' clustering index (i.e., $I_M = 0$) evolved over time (Figure S3). One type of simulation was a "deterministic simulation" in which each cell exactly sensed the concentration of the signaling molecule without making errors (Figure 5C). Another type of simulation was a "stochastic simulation" in which the cells made errors in sensing the concentration of the signaling molecule (Figures S4 and S5). Both types of simulations are similar in spirit to the cellular automata and Ising-type models that researchers have previously used in studying pattern formation in developmental and neuronal systems (Ermentrout and Edelstein-Keshet, 1993; Hopfield, 1982). In both types of simulations, we discovered that if nearly 50% of the cells are initially ON and they are in the "activation-deactivation" region (Figure 5C, white region in phenotype diagram), then a spatially disordered

population of cells (i.e., $I_M \sim 0$) has a higher chance of evolving into a population with spatially ordered patterns (i.e., I_M closest to 1) than if the cells were in the activation region or the deactivation region (Figure 5C, compare the three graphs of I_M) (also see Figures S4, S5, and S6). Intuitively, this occurs because for a spatially disordered population to be spatially ordered the randomly scattered OFF cells and ON cells need to expand or contract their territories to form consolidated islands of OFF and ON cells, respectively. The expansion of OFF (and ON) cells requires deactivation (and activation), which enables a clustered region of OFF (and ON) cells to cooperatively create more OFF (and ON) cells in their adjacent regions. Such dynamic regulations of the shape and size of the OFF and ON regions are required to form islands of highly clustered OFF and ON cells. Thus, when the activation and deactivation co-exist, both ON and OFF cells can simultaneously regulate their shapes and sizes. This enables a spatially disordered population to evolve into a population with a higher spatial order, more so than when activation alone or deactivation alone is present.

We also observed in our simulations that some spatially disordered populations could maintain their fraction of ON cells at a nearly constant value over time while sharply increasing their spatial ordering (i.e., increasing the I_M to a high value near 1). This resulted in highly defined and striking spatial patterns (highly ordered stripes and islands of ON cells) that are stable for long periods of time (Figure S6). The ordered spatial patterns formed if the cells were in the activation-deactivation region of the phenotype diagram. The entropy of population forms a landscape as a function of the threshold concentration K and the maximal concentration S_{ON} (height of the landscape is represented as a heat map in Figure 5B). This landscape has a minimal basin (i.e., a region of local minimum for the entropy of population) within the activation-deactivation region (Figure 5B, lower). In our simulations, we found that cells in this region of minimal entropy formed the most stable and ordered spatial patterns (Figure S6). Moreover, we observed that spatial clustering of cells strongly influences how the ON/OFF state of each cell in a population changes over time (see Supplemental Theoretical Procedures and Figure S7).

In summary, our results show that our quantification of degrees of autonomy and of collectiveness is meaningful in making sense of population-level dynamics, including genetically identical cells self-organizing into defined spatial patterns of the types that we encounter in animal development. In particular, our results reveal that a decrease in the entropy of population accompanied by a strong signaling strength, which creates the activation-deactivation region, is correlated with the cells forming highly ordered spatial patterns (Figure 5C).

DISCUSSION

On a conceptual level, we have shown that the cells' degrees of autonomy and of collectiveness—two concepts that are central to all multicellular behaviors that are typically loosely and qualitatively treated—can be sensibly defined, quantified, and tuned. This has practical implications. For example, the gain of autonomy by a few renegade secrete-and-sense cells in a healthy tissue often marks the beginnings of a tumor growth (e.g., renegade secreting-and-sensing of IL-6 by a few cells trigger breast carcinoma) (Sansone et al., 2007; Sporn and Todaro, 1980). Thus, quantifying an increase in the autonomy and the decrease in the collectiveness of cells may provide quantitative insights into how tumors arise. Our theory may also aid in quantitatively analyzing how maintaining collectiveness keeps tissues healthy.

On a practical level, our work identified the interconnected relationships among the components of genetic circuits and cell-cell signaling that experimentalists can tune to control the cells' autonomous and collective behaviors. We also identified what these behaviors are. The behaviors can be any features of cells that our idealized ON/OFF genes influence downstream. Cells can tune their threshold concentration, for example, by changing the production level of a transcription factor that mediates the positive or negative feedback (Youk and Lim, 2014) or by changing the abundance of the receptors that bind the signaling molecule (e.g., epidermal growth factor [EGF] receptor in EGF signaling) (DeWitt et al., 2001). Cells can tune their signaling length, for example, by secreting a protease that degrades the signaling molecule (e.g., Bar1 in budding yeast, Rappaport and Barkai, 2012; Diener et al., 2014; phosphodiesterase in the soil amoebae *D. discoideum*, Gregor et al., 2010). Our work shows that varying the geometric shape of tissues or organs composed of secreting-and-sensing cells can also tune their signaling length. Researchers have experimentally shown many other ways of tuning these elements (Hart et al., 2014; Sgro et al., 2015; Gregor et al., 2010). Thus, our theory provides a readily applicable and common framework for understanding and engineering diverse multicellular systems composed of secrete-and-sense cells. Our results for the cells with binary gene regulation (Figures 1D and 1E) also apply to cells that have a finite Hill coefficient controlling their positive or negative feedbacks (see Supplemental Theoretical Procedures and Figures S8, S9, and S10).

Our work also suggests the underappreciated ability of secrete-and-sense cells to generate defined spatial patterns, akin to those seen in development of animals such as the fruit fly (e.g., via secreting-and-sensing Wingless) (Hooper, 1994). Specifically, our work shows that given an initial arrangement of ON and OFF secrete-and-sense cells that is spatially disordered, it is possible for highly ordered spatial patterns such as stripes and islands of ON/OFF cells to emerge, with the caveat that the exact location of the spatial patterns in the field of cells is determined by the initial locations of the ON and OFF cells. Thus, if another mechanism sets up a particular initial pattern, which can be spatially disordered (i.e., $I_M \sim 0$), cell-cell communication among the secrete-and-sense cells can take over and generate highly ordered spatial patterns. This may suggest that tissues and embryos composed of secrete-and-sense cells are ideal candidates for realizing the "Turing-like" patterning mechanism (Turing, 1952). Despite decades of search for multicellular systems that use a patterning mechanism similar to the one proposed by Turing, it has been difficult to conclusively prove in many systems that the observed spatial patterns originate from Turing's mechanism (Economou et al., 2012). The main difficulty has been that Turing's formulation of spatial patterning (Turing, 1952) involves only molecules (activator and inhibitor) but not cells. We suggest that it might be fruitful to investigate how secrete-and-sense cells in the activation-deactivation region of the phenotype diagram (Figure 4C), despite not satisfying

exactly the conditions of Turing's activator and inhibitor molecules, may act a cellular analogs of Turing's activators and inhibitors.

We also note that the entropy of population σ describes how many spatial patterns can be stably sustained in a population and can be rigorously defined even if the only information we have about the population is the values of the three molecular parameters, S_{ON}, K, and L, without knowing anything else. Without knowing anything about the initial ON/OFF state of every or even any cell in the population, the entropy of population will predict precisely how many spatial patterns can arise in the population and how likely it is that these patterns are spatially ordered (through the relationship between σ and the spatial clustering index I_M). Being able to predict a population-level property without having detailed information about the state of any individual cell makes the entropy of population similar in spirit to the thermodynamic entropy (Landau and Lifshitz, 1980) and the Shannon's informational entropy (Shannon, 1948), both of which quantify a systems-level property without having information about the detailed microstate of the system. Thus, the entropy of population allows one to predict how likely the expression level of a gene (e.g., ON/OFF) in each cell in a population would form a spatially ordered pattern, in cases where we cannot experimentally measure the expression levels of a gene in any cell in multicellular systems such as a tissue or a biofilm. This connection between the entropy of population and spatial order is reminiscent of the link between the thermodynamic entropy and the amount of disorder in a physical system and also of the link between randomness of information in a message and the Shannon informational entropy. It may be fruitful to investigate whether there are deeper connections between Shannon's entropy and the entropy of population, given that both deals with how much information is accessible to an experimentalist about a particular system.

We hope that our work will motivate future studies that use first principles to link genetic circuits with multicellular behaviors. Future works that explore alternative ways of defining and quantifying degrees of autonomy and collectiveness in other types of cells will, together with our theory, provide a rigorous framework for understanding and manipulating multicellular systems. As we have done here, such studies will reveal how quantitative principles of macroscopic living systems emerge from the microscopic laws of molecular and cellular interactions (Phillips, 2015; Mehta and Gregor, 2010; Perrimon and Barkai, 2011).

THEORETICAL PROCEDURES

Basic Unit: Boundaries of Phenotypes

The boundaries within the activation and the deactivation regions for the basic unit (Figure 4A) are given by $A_n(K,S_{ON},L)$ and $D_n(K,S_{ON},L)$, respectively,

$$A_n(K,S_{ON},L)=S_{ON}-\frac{1}{ne^{-1/L}}K+\frac{1+(6-n)e^{-1/L}}{ne^{-1/L}},\quad n=1...6 \tag{Equation 9}$$

$$D_n(K,S_{ON},L)=S_{ON}-\frac{1}{1+ne^{-1/L}}K+\frac{(6-n)e^{-1/L}}{1+ne^{-1/L}},\quad n=1...6,$$

with $A_0(K,S_{ON},L)=-K+1+6e^{-1/L}$ and $D_0(K,S_{ON},L)=S_{ON}-K+6e^{-1/L}$. Details are in the Supplemental Theoretical Procedures.

Population with *N* Cells: Boundaries of Phenotypes

With the A_n and D_n defined as above, the boundaries in the phenotype diagram for N cells (Figure 4C) are

$$\begin{cases} A_0(K,S_{ON},L)=1+f_N(L)-K \\ A_{N-1}(K,S_{ON},L)=S_{ON}+\dfrac{1-K}{f_N(L)} \\ D_0(K,S_{ON},L)=S_{ON}-K+f_N(L) \\ D_{N-1}(K,S_{ON},L)=S_{ON}-\dfrac{K}{1+f_N(L)} \end{cases}. \tag{Equation 10}$$

Definition of the Clustering Index

We define a clustering index I_M that quantifies how closely ON cells (and thus OFF cells) are clustered together in space:

$$I_M\equiv\left[\frac{1}{\sum_{i=1}^{N}\sum_{j=1}^{N}w_{ij}}\sum_{i=1}^{N}\sum_{j=1}^{N}w_{ij}(C_i-\overline{C})(C_j-\overline{C})\right]\frac{N}{\sum_{i=1}^{N}(C_i-\overline{C})^2}. \tag{Equation 11}$$

Here r_{ij} is the distance between i^{th} and j^{th} cells and $w_{ij}\equiv 1/r_{ij}$. C_n is the state of n^{th} cell and $\overline{C}$ is the average of all the C_ns. I_M can be between 0 (spatially disordered) and 1 (spatially ordered).

SUPPLEMENTAL INFORMATION

Supplemental Information includes Supplemental Theoretical Procedures and ten figures and can be found with this article online at http://dx.doi.org/10.1016/j.cels.2015.10.012.

AUTHOR CONTRIBUTIONS

T.M. and H.Y. designed the research. T.M. performed the research with guidance from H.Y. Both authors wrote the manuscript.

ACKNOWLEDGMENTS

We thank E. Helguero, B. Doganer, A. Ravensbergen, D. Alvarez, H. Le Chenadec, and A. Raj for insightful suggestions. H.Y. is partially supported by a NWO NanoFront Grant.

Received: July 23, 2015
Revised: October 6, 2015
Accepted: October 29, 2015
Published: November 25, 2015

REFERENCES

Ben-Zvi, D., Shilo, B.-Z., Fainsod, A., and Barkai, N. (2008). Scaling of the BMP activation gradient in Xenopus embryos. Nature *453*, 1205–1211.

Chen, C.C., Wang, L., Plikus, M.V., Jiang, T.X., Murray, P.J., Ramos, R., Guerrero-Juarez, C.F., Hughes, M.W., Lee, O.K., Shi, S., et al. (2015). Organ-level quorum sensing directs regeneration in hair stem cell populations. Cell *161*, 277–290.

Dayarian, A., Chaves, M., Sontag, E.D., and Sengupta, A.M. (2009). Shape, size, and robustness: feasible regions in the parameter space of biochemical networks. PLoS Comput. Biol. *5*, e1000256.

DeWitt, A.E., Dong, J.Y., Wiley, H.S., and Lauffenburger, D.A. (2001). Quantitative analysis of the EGF receptor autocrine system reveals cryptic regulation of cell response by ligand capture. J. Cell Sci. *114*, 2301–2313.

Diener, C., Schreiber, G., Giese, W., del Rio, G., Schröder, A., and Klipp, E. (2014). Yeast mating and image-based quantification of spatial pattern formation. PLoS Comput. Biol. *10*, e1003690.

Economou, A.D., Ohazama, A., Porntaveetus, T., Sharpe, P.T., Kondo, S., Basson, M.A., Gritli-Linde, A., Cobourne, M.T., and Green, J.B. (2012).

Periodic stripe formation by a Turing mechanism operating at growth zones in the mammalian palate. Nat. Genet. *44*, 348–351.

Ermentrout, G.B., and Edelstein-Keshet, L. (1993). Cellular automata approaches to biological modeling. J. Theor. Biol. *160*, 97–133.

Fallon, E.M., and Lauffenburger, D.A. (2000). Computational model for effects of ligand/receptor binding properties on interleukin-2 trafficking dynamics and T cell proliferation response. Biotechnol. Prog. *16*, 905–916.

Govern, C.C., and ten Wolde, P.R. (2012). Fundamental limits on sensing chemical concentrations with linear biochemical networks. Phys. Rev. Lett. *109*, 218103.

Gregor, T., Bialek, W., de Ruyter van Steveninck, R.R., Tank, D.W., and Wieschaus, E.F. (2005). Diffusion and scaling during early embryonic pattern formation. Proc. Natl. Acad. Sci. USA *102*, 18403–18407.

Gregor, T., Tank, D.W., Wieschaus, E.F., and Bialek, W. (2007). Probing the limits to positional information. Cell *130*, 153–164.

Gregor, T., Fujimoto, K., Masaki, N., and Sawai, S. (2010). The onset of collective behavior in social amoebae. Science *328*, 1021–1025.

Hart, Y., and Alon, U. (2013). The utility of paradoxical components in biological circuits. Mol. Cell *49*, 213–221.

Hart, Y., Antebi, Y.E., Mayo, A.E., Friedman, N., and Alon, U. (2012). Design principles of cell circuits with paradoxical components. Proc. Natl. Acad. Sci. USA *109*, 8346–8351.

Hart, Y., Reich-Zeliger, S., Antebi, Y.E., Zaretsky, I., Mayo, A.E., Alon, U., and Friedman, N. (2014). Paradoxical signaling by a secreted molecule leads to homeostasis of cell levels. Cell *158*, 1022–1032.

Hermsen, R., Ursem, B., and ten Wolde, P.R. (2010). Combinatorial gene regulation using auto-regulation. PLoS Comput. Biol. *6*, e1000813.

Hooper, J.E. (1994). Distinct pathways for autocrine and paracrine Wingless signalling in Drosophila embryos. Nature *372*, 461–464.

Hopfield, J.J. (1982). Neural networks and physical systems with emergent collective computational abilities. Proc. Natl. Acad. Sci. USA *79*, 2554–2558.

Lalanne, J.-B., and François, P. (2015). Chemodetection in fluctuating environments: receptor coupling, buffering, and antagonism. Proc. Natl. Acad. Sci. USA *112*, 1898–1903.

Landau, L.D., and Lifshitz, E.M. (1980). Statistical Physics, *Volume 5*, Third Edition (Butterworth-Heinemann).

Long, T., Tu, K.C., Wang, Y., Mehta, P., Ong, N.P., Bassler, B.L., and Wingreen, N.S. (2009). Quantifying the integration of quorum-sensing signals with single-cell resolution. PLoS Biol. *7*, e68.

Markson, J.S., and Elowitz, M.B. (2014). Synthetic biology of multicellular systems: new platforms and applications for animal cells and organisms. ACS Synth. Biol. *3*, 875–876.

Martinez Arias, A., and Stewart, A. (2002). Molecular Principles of Animal Development (New York: Oxford University Press).

Mehta, P., and Gregor, T. (2010). Approaching the molecular origins of collective dynamics in oscillating cell populations. Curr. Opin. Genet. Dev. *20*, 574–580.

Mehta, P., Goyal, S., Long, T., Bassler, B.L., and Wingreen, N.S. (2009). Information processing and signal integration in bacterial quorum sensing. Mol. Syst. Biol. *5*, 325.

Moran, P.A.P. (1950). Notes on continuous stochastic phenomena. Biometrika *37*, 17–23.

Ng, W.L., and Bassler, B.L. (2009). Bacterial quorum-sensing network architectures. Annu. Rev. Genet. *43*, 197–222.

Pai, A., and You, L. (2009). Optimal tuning of bacterial sensing potential. Mol. Syst. Biol. *5*, 286.

Pai, A., Tanouchi, Y., and You, L. (2012). Optimality and robustness in quorum sensing (QS)-mediated regulation of a costly public good enzyme. Proc. Natl. Acad. Sci. USA *109*, 19810–19815.

Pai, A., Srimani, J.K., Tanouchi, Y., and You, L. (2014). Generic metric to quantify quorum sensing activation dynamics. ACS Synth. Biol. *3*, 220–227.

Payne, S., Li, B., Cao, Y., Schaeffer, D., Ryser, M.D., and You, L. (2013). Temporal control of self-organized pattern formation without morphogen gradients in bacteria. Mol. Syst. Biol. *9*, 697.

Perrimon, N., and Barkai, N. (2011). The era of systems developmental biology. Curr. Opin. Genet. Dev. *21*, 681–683.

Perrimon, N., Pitsouli, C., and Shilo, B.-Z. (2012). Signaling mechanisms controlling cell fate and embryonic patterning. Cold Spring Harb. Perspect. Biol. *4*, a005975.

Phillips, R. (2015). Napoleon is in equilibrium. Annu. Rev. Condens. Matter Phys. *6*, 85–111.

Rappaport, N., and Barkai, N. (2012). Disentangling signaling gradients generated by equivalent sources. J. Biol. Phys. *38*, 267–278.

Sansone, P., Storci, G., Tavolari, S., Guarnieri, T., Giovannini, C., Taffurelli, M., Ceccarelli, C., Santini, D., Paterini, P., Marcu, K.B., et al. (2007). IL-6 triggers malignant features in mammospheres from human ductal breast carcinoma and normal mammary gland. J. Clin. Invest. *117*, 3988–4002.

Savir, Y., Waysbort, N., Antebi, Y.E., Tlusty, T., and Friedman, N. (2012). Balancing speed and accuracy of polyclonal T cell activation: a role for extracellular feedback. BMC Syst. Biol. *6*, 111.

Sgro, A.E., Schwab, D.J., Noorbakhsh, J., Mestler, T., Mehta, P., and Gregor, T. (2015). From intracellular signaling to population oscillations: bridging size- and time-scales in collective behavior. Mol. Syst. Biol. *11*, 779.

Shannon, C.E. (1948). A mathematical theory of communication. Bell Syst. Tech. J. *27*, 379–423.

Song, H., Payne, S., Gray, M., and You, L. (2009). Spatiotemporal modulation of biodiversity in a synthetic chemical-mediated ecosystem. Nat. Chem. Biol. *5*, 929–935.

Sporn, M.B., and Todaro, G.J. (1980). Autocrine secretion and malignant transformation of cells. N. Engl. J. Med. *303*, 878–880.

Sprinzak, D., Lakhanpal, A., Lebon, L., Santat, L.A., Fontes, M.E., Anderson, G.A., Garcia-Ojalvo, J., and Elowitz, M.B. (2010). Cis-interactions between Notch and Delta generate mutually exclusive signalling states. Nature *465*, 86–90.

Tanouchi, Y., Tu, D., Kim, J., and You, L. (2008). Noise reduction by diffusional dissipation in a minimal quorum sensing motif. PLoS Comput. Biol. *4*, e1000167.

Turing, A.M. (1952). The chemical basis of morphogenesis. Philos. Trans. R. Soc. Lond., B *237*, 37–72.

You, L., Cox, R.S., 3rd, Weiss, R., and Arnold, F.H. (2004). Programmed population control by cell-cell communication and regulated killing. Nature *428*, 868–871.

Youk, H., and Lim, W.A. (2014). Secreting and sensing the same molecule allows cells to achieve versatile social behaviors. Science *343*, 1242782.